crystals

MDPI

Article

Effect of Varying Hot Extrusion Temperatures on the Properties of a Sinterless Turning Induced Deformation Processed Eco-Friendly Mg-Zn-Ca Alloy

Zhipeng Wang, Gururaj Parande and Manoj Gupta *

Department of Mechanical Engineering, National University of Singapore, 9 Engineering Drive 1, Singapore 117576, Singapore
* Correspondence: mpegm@nus.edu.sg; Tel.: +65-6516-6358

Abstract: In this work, Mg-4Zn-1Ca (wt. %) alloy was primarily processed by disintegrated melt deposition. The resulting ingots were further pre-processed by the turning induced deformation technique (TID), and the turnings were subsequently consolidated by the hot extrusion process and sinterless powder metallurgy. A range of extrusion temperatures (200, 250 and 300 °C) was tested to understand the effect of the extrusion temperature on tailoring the microstructure and properties of TID-processed Mg-4Zn-1Ca (wt. %) alloys. The results indicated that the combined effect of TID and extrusion temperature plays a significant role in grain refinement, specifically at 200 °C. Overall, the sample extruded at 300 °C showed the best microhardness and compressive yield strength values. The resistance to ignition and wet corrosion increased and decreased, respectively, when the extrusion temperature was increased. Variations of basal texture and fine grain strengthening due to variations of extrusion temperature led to different properties peaking at different extrusion temperatures. Microstructure-property relationships are therefore discussed, highlighting that different extrusion temperatures have characteristic effects in improving and lowering the properties. Many of the investigated properties of TID-processed alloys exceed that of commercial Mg alloys, suggesting the capability of the sinterless TID technique to develop as an economical industrial way of recycling and manufacturing magnesium-based materials.

Keywords: magnesium alloy; TID (turning induced deformation); hybrid manufacturing; hot extrusion; powder metallurgy; mechanical properties; thermal behavior; corrosion behavior

Citation: Wang, Z.; Parande, G.; Gupta, M. Effect of Varying Hot Extrusion Temperatures on the Properties of a Sinterless Turning Induced Deformation Processed Eco-Friendly Mg-Zn-Ca Alloy. *Crystals* **2023**, *13*, 3. https://doi.org/10.3390/cryst13010003

Academic Editor: Bolv Xiao

Received: 21 November 2022
Revised: 9 December 2022
Accepted: 16 December 2022
Published: 20 December 2022

1. Introduction

Magnesium (Mg) and its alloys exhibit high specific strength and high specific stiffness, thereby attracting much interest from engineers and scientists. Owing to their lightweight property, magnesium alloys are widely used in weight-critical applications particularly in transportation sectors [1–3]. Further, magnesium alloys are ideal candidate materials for bone tissue engineering due to their controlled degradability, high room temperature mechanical strength, and adequate biocompatibility [4]. Additionally, the mechanical properties and physical properties such as density and elastic modulus of magnesium alloys are very similar to that of natural bone. This contributes to the reduction of stress-shielding issues, whereby the implant will bear most of the load instead of the surrounding bones leading to the degradation and resorption of bone [5,6]. This is the key differentiating factor when compared to incumbent biometals such as titanium and stainless steel.

Pure Mg is not suitable for orthopedic applications as it undergoes rapid degradation that results in the accumulation of hydrogen gas bubbles and subsequent loss of mechanical strength over time. Alloying is the most common method for improving the mechanical properties and corrosion resistance performance of magnesium [7]. Many alloying elements, such as aluminum (Al), zinc (Zn), calcium (Ca), zirconium (Zr), and rare earths (RE), have been widely used to improve the properties and corrosion resistance. However, Al is

considered neurotoxic, while RE elements display long-term cytotoxicity, making them unviable for use in orthopedic implant applications [8]. Less potentially toxic effects on the human body are induced by Zn and Ca during their degradation [9]. Moreover, the addition of Zn and Ca contributes to the weakening of the strong texture associated with Mg [10]. With an increasing amount of Zn, the static recrystallization process is accelerated due to the decreasing grain boundary energy and the increase in nucleation, leading to the simultaneous increment of uniform elongation and post-uniform elongation [10]. Zinc can also promote the formation of the Mg-Zn-Ca ternary phase, leading to the improvement in the mechanical strength and corrosion resistance with the increase in the Zn/Ca atom ratio. Additions of Ca also showed the improvement of flame-retardant properties and improvement in the machinability of magnesium alloy [11]. The Mg-Zn-Ca system is considered reasonable for medical applications due to its excellent mechanical properties and biocompatibility [12–14].

In comparison with other light metals, magnesium and its alloys show good machinability, including good surface finish, lower energy costs, less tool wear, smaller cutting force, faster-cutting speed capability, and better swarf quality [15–17]. Therefore, magnesium alloys are generally conducive to being processed by different machining processes. However, a lot of chips are generated during machining, which are often discarded or remelted to recover magnesium alloys, leading to material losses and higher energy costs. TID (Turning Induced Deformation) technology is an efficient, energy-saving, and low-cost magnesium recycling technology [18–20]. This technology consolidates the chips generated in the turning process of magnesium and its alloys. In the TID process, chips are collected during turning (when the deformation induced by turning occurs) under certain fixed machining parameters, subsequently cold, compacted, and hot extruded conditions. This technique has been introduced into the recycling of various metals such as aluminum and copper [21], and the impact of varying turning parameters such as turning speed and depth of cut on the microstructure and mechanical properties of magnesium alloy was studied [19]. The plastic deformation induced by turning contributes to the improvement in the properties of magnesium alloy by deformation strengthening. Compared with the materials processed by the traditional machining method, mechanical strength, micro-hardness and damping properties of magnesium alloy processed by the TID are found to be significantly improved [18]. The studies on TID technology provide a feasible processing route to obtain high-performance magnesium alloys using a high material utilization energy-efficient method, which has very important economic and environmental significance. In magnesium, Tekumalla et al. [19] analyzed the effect of cutting speed on the microstructure and mechanical properties of ZK60 magnesium alloys. The findings showed that low turning speed would lead to the generation of discontinuous chips, resulting in the final magnesium alloy with lower porosity and smaller grain size, which not only improved the strength of the material without affecting the ductility but also improved the ignition point and damping properties. Tekumalla et al. [20] analyzed the impact of cutting depth in TID technology on the mechanical properties and microstructure of AZ91 magnesium alloy materials which revealed that the larger cutting depth causes the larger plastic deformation of the chip, which ultimately improved the hardness and compressive strength of the material. The dynamic recrystallization process during hot extrusion plays a decisive role in the density, microstructure, and mechanical properties of the final magnesium alloy. However, the current research mainly focuses on the turning process of TID technology, and there is a lack of research on the influencing factors in the primary processing conditions, such as the hot extrusion temperatures, hot extrusion ratios, hot extrusion pressures, and compaction pressures.

Accordingly, in this study, an attempt was made to understand the influence of varying extrusion temperatures (200 °C, 250 °C and 300 °C) on the structure and performance of TID-based eco-friendly magnesium alloy (Mg-4Zn-1Ca). The physical, thermal, mechanical, and corrosion properties of the obtained billets were determined to explore the feasibility of being used for both structural and orthopedic applications.

2. Materials and Methods

2.1. Processing

In this work, magnesium turnings supplied by ACROS Organics, Waltham, MA, USA (purity > 99%) and zinc powder (purity > 98.5%, size ~100 μm) and calcium granules (purity > 99%) supplied by Alfa Aesar, Ward Hill, MA, USA were used to synthesize the alloy using the Disintegrated Melt Deposition (DMD) method. Raw material (magnesium turnings, zinc powder, and calcium granules) was laid out in layers in the graphite crucible with argon shielding gas and heated to 750 °C to melt all the raw materials. The melt was stirred at 450 rpm for 5 min to ensure the uniform mixing of the raw materials and homogenization of temperature. The molten metal was then disintegrated under the action of argon jets and bottom-poured into a 40 mm diameter mold and cooled to room temperature. The billet was subsequently subjected to the TID (turning induced deformation) technique employing a turning speed of 55 mm/min and a depth of cut of 1 mm. Chips were carefully collected to prevent foreign impurities and possible oxidation. The collected chips were cold compressed at a pressure of 600 psi (4.13 MPa). It is worth noting that no sintering was performed after the compaction of the billets. The compact billets were hot extruded at 200 °C, 250 °C, and 300 °C at an extrusion ratio of 20.25:1 to yield cylindrical rods of 8 mm in diameter.

2.2. Characterization

The experimental density of the samples was calculated using the Archimedes principle. Samples were weighed in both air and distilled water using two electronic balances (Setra EL-4100S for air, A&D GR-200 for water) ten times with an error of ±0.0001 g to determine an average mass in both air and water. The theoretical density was determined using the rule of mixtures. Porosity values are calculated using the theoretical and experimental densities.

Grain size analysis was performed using the Leica DM 2500M optical microscope. JEOL JSM-5800 LV Scanning Electron Microscope (SEM) was used to observe and analyze the sample surface to determine the distribution of the secondary phase. Possible second phases were further analyzed using X-ray diffraction (XRD). The samples are exposed to X-ray radiation (Cu Kα; λ = 1.54056 A°) while an automated diffractometer (Shimadzu Lab-XRD-6000) was used with a scan speed of 2°/min to detect the diffraction signal.

The phase transition temperature was measured by Shimadzu differential scanning calorimeter (DSC-60). The sample was placed in a flowing argon atmosphere and heated uniformly (5 °C/min) from 30 °C to 600 °C.

A thermogravimetric analyzer was used to determine the ignition temperature. In thermogravimetric analysis (TGA), the samples were placed in purified air with a flow rate of 50 mL/min. The samples were heated uniformly (10 °C/min) from 25 °C to 900 °C.

The coefficient of thermal expansion (CTE) of the three groups of samples was measured by a Linseis TMA PT1000LT thermomechanical analyzer. The sample was placed in a protective argon atmosphere with a flow rate of 0.1 L/min. The sample was slowly heated (5 °C/min) from 25 °C to 600 °C, and the displacement (thermal expansion) of the sample as a function of temperature was recorded.

According to ASTM standard E34-08, a Vickers hardness tester was used to measure the microhardness. An automatic digital micromechanical tester (Shimadzu HMV) with a Vickers indenter was used at a total load of 490.3 mN (±0.05 HV) and dwell time of 15 s. Twenty measurements were performed per sample.

The samples were also tested for quasi-static compression following ASTM standard test method E9-89A. Samples of 8 mm in diameter and 8 mm in length were tested using the MTS-810 servo-hydraulic test machine at a strain rate set at 4×10^{-3}/s. The strain-stress curve was recorded and analyzed to obtain compressive yield strength (CYS), ultimate compressive strength (UCS) and fracture strain of all the samples. A scanning electron microscope (JEOL JSM-5800 LV) was used to observe the fracture surfaces to analyze the failure mechanism.

The samples were cut into ~50 mm in length and ~8 mm in diameter for the damping measurements. Manual excitation was used in the test and the vibration signals were detected and recorded by resonant frequency and damping analyzer (RFDA) equipment (IMCE, Belgium). Through the relationship between the vibration signal and time, the damping coefficient and Young's modulus were recorded.

To study the corrosion resistance properties of the material in the human body, samples of ~5 mm in diameter and ~5 mm in length were immersed in Hank's Balanced Salt Solution (HBSS) (From Lonza Chemicals Pte Ltd. Singapore) with a ratio of solution volume to the surface area of samples 20 mL:1 cm^2. The whole device was installed in a 37 °C constant temperature water bath to simulate the human body temperature. The corrosion experiment lasted for seven days. On the first three days and last day, the samples are taken out and cleaned with a mixture of chromium trioxide (CrO_3) and silver nitrate ($AgNO_3$) solution and then the weight of the soaked samples and the pH of the HBSS solution were recorded. To eliminate human interference, the control group was not operated, and the weight loss and pH values were recorded after seven days.

3. Results and Discussion

3.1. Density and Porosity

The experimental density and porosity of the TID-based magnesium alloys are shown in Table 1. The porosity of the samples using TID technology is comparable to that of no TID sample. The porosity increases with the increase in extrusion temperature. When the temperature rises from 200 °C to 250 °C, the porosity increases noticeably (0.68 to 1.01%), but minimally when the temperature rises from 250 °C to 300 °C (1.01 to 1.02%). The porosity evolves due to the entrapment of oxygen between the chip voids during the compaction process. Further, the compaction pressure used in the study is 600 psi (4.13 MPa), lower than the traditionally used 1000 psi (6.89 MPa) for Mg alloys [22]. For near-dense magnesium materials, a porosity < 2% is industrially acceptable. Overall, the TID samples display lower levels of porosity owing to the optimized TID, compaction and extrusion parameters selected for the study.

Table 1. Density and porosity results.

Processing Conditions	Experimental Density (g/cm^3)	Porosity (%)
No TID (250 °C)	1.763 ± 0.002	1.22
200 °C	1.7726 ± 0.005	0.68
250 °C	1.7667 ± 0.007	1.01
300 °C	1.7666 ± 0.002	1.02

3.2. Microstructure

The grain size results are shown in Table 2 and their representative microstructural images are shown in Figure 1. The high extrusion ratio used in the study leads to a dynamic recrystallization (DRX) effect, as evidenced by Figure 1b,d,f. Two distinct phases can be found in the micrographs that of the magnesium matrix and a phase containing magnesium, zinc, and calcium. The fine MgZnCa phase appears segregated along the direction parallel to the extrusion direction and was observed along the grain boundaries, as seen in Figure 1. Microstructural observations also revealed that the grains near the phases exhibited a finer grain size. Due to the low fault energy of magnesium alloy, dynamic recrystallization is easy to occur in Mg-4Zn-1Ca alloys during hot deformation [20,23]. This is attributed to the fact that under the action of extrusion load, many dislocations are formed and forced to move, resulting in plastic deformation. However, because of the limited slip systems in the magnesium matrix, the dynamic recovery process inside the material remains slow [24]. At a certain temperature, nucleation and recrystallization can occur. In addition, the dislocations are subjected to entangling and locking, which increased the local dislocation density and provides the necessary crystal nuclei and energy

for recrystallization [25]. Similarly, when using the turning-induced deformation (TID) technology, the chips underwent plastic deformation and formed several dislocations, which increase the nucleation speed of dynamic recrystallization during extrusion and enhanced the fine grain strengthening effect of dynamic recrystallization as shown in Table 2.

Table 2. Grain size results.

Processing Conditions	Grain Size (μm)
No TID (250 °C)	4.9 ± 1.3
200 °C	1.1 ± 0.4
250 °C	3.8 ± 1.1
300 °C	4.5 ± 1.4

The recrystallization process closely governs the related microstructure and mechanical properties of the TID-processed Mg-4Zn-1Ca alloy. In Figure 1, coarse columnar grains and fine equiaxed grains formed by dynamic recrystallization can be simultaneously seen to highlight the bimodal nature of the grain refinement. This indicates that incomplete dynamic recrystallization occurs during extrusion. With the increase in temperature, the atomic diffusion coefficient becomes larger, which will promote grain boundary migration and grain growth [26]. Hence, the microstructure with a smaller average grain size is obtained at a lower extrusion temperature. The recrystallization process tends to be complete at a higher extrusion temperature, and the grain size becomes larger and uniform.

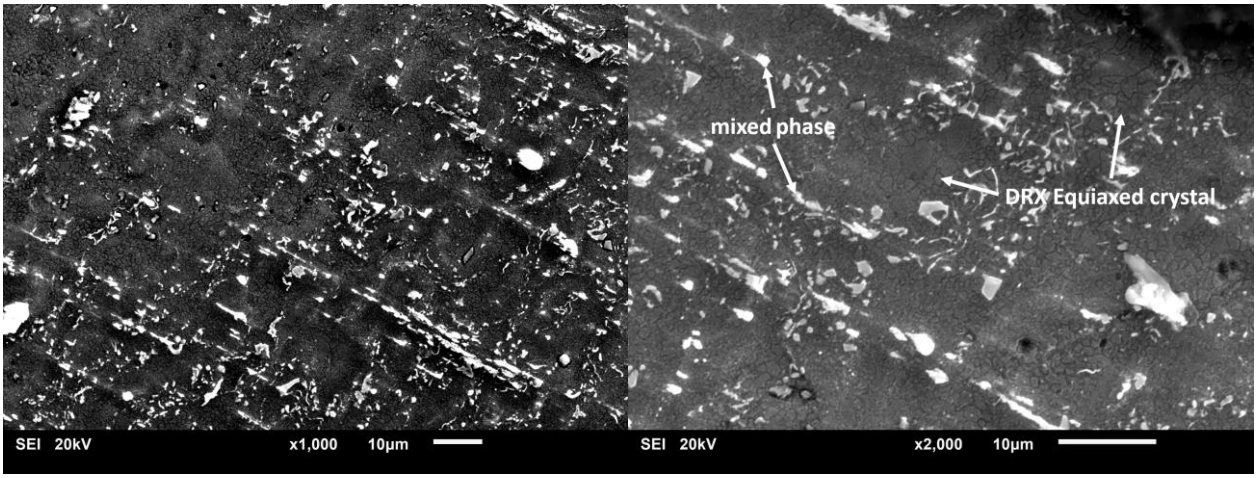

(**a**) (**d**)

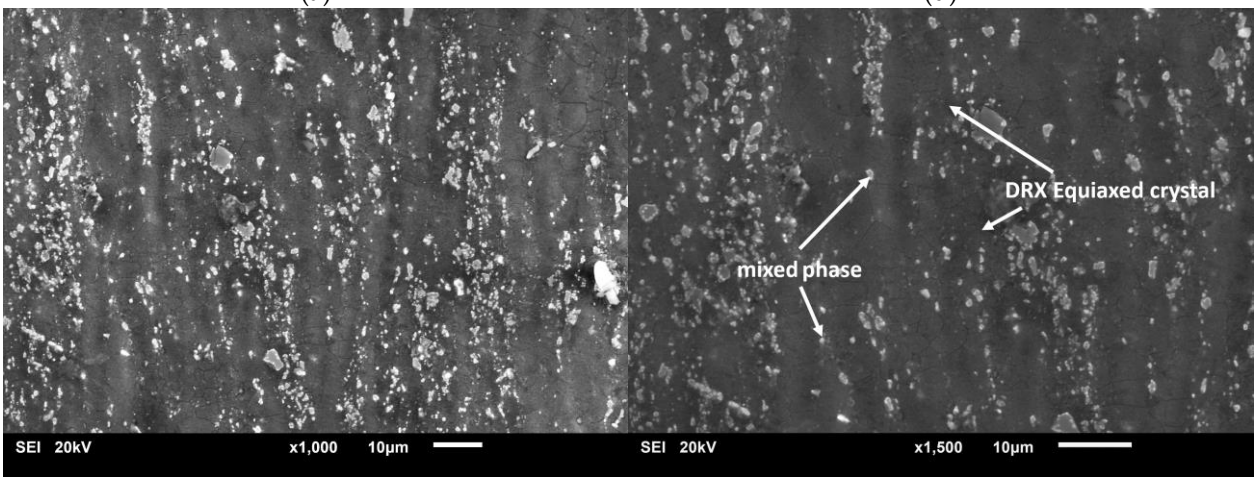

(**b**) (**e**)

Figure 1. *Cont.*

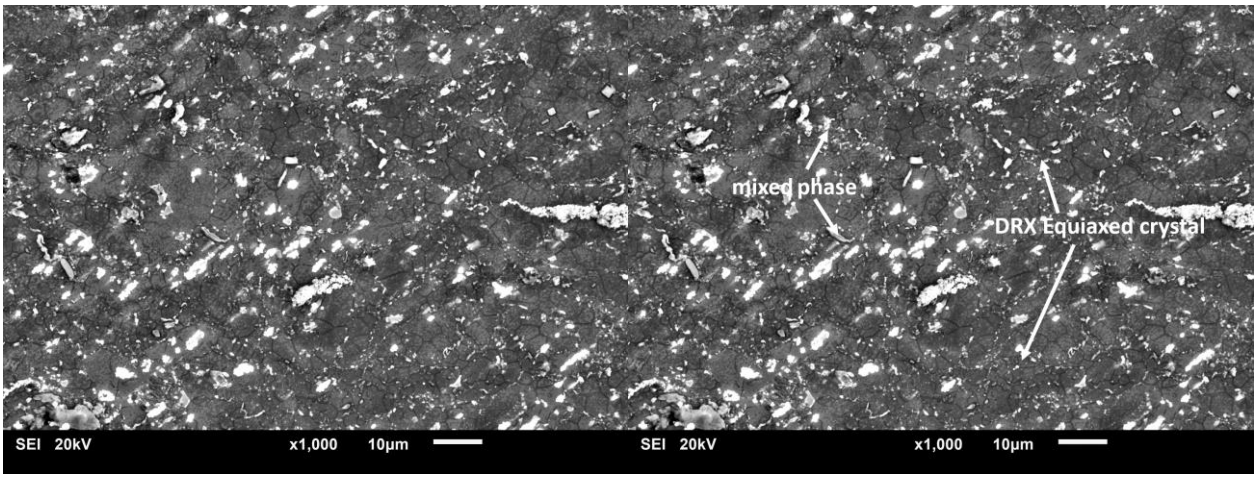

(**c**) (**f**)

Figure 1. Scanning electron microscopy (SEM) graphs of different samples along the longitudinal section. (**a**,**d**) 200 °C; (**b**,**e**) 250 °C; (**c**,**f**) 300 °C.

The identity of these phases was further confirmed using X-ray diffraction (XRD) analysis. Figure 2 shows the XRD results, which reveal the presence of magnesium matrix and zinc oxide (ZnO). The characteristic peaks observed at 2θ = 32°, 34° and 36° in the graphs correspond to the (1010) prismatic, (0002) basal, and (1011) pyramidal planes of HCP Mg crystal. The characteristic peaks of ZnO can also be found at 2θ = 32°, 34°, and 36° with (100), (002), and (101) planes. $Mg_{0.97}Zn_{0.03}$ and $Ca_2Mg_6Zn_3$ have a characteristic peak at 2θ = 36°, and $Mg_{0.97}Zn_{0.03}$ also has a characteristic peak at 2θ = 57°, respectively, which proves their presence albeit with very little content. The XRD results also showed the possibility of minimal amounts of other metal oxide phases during the TID process (including calcium oxide (CaO) and magnesium oxide (MgO)) from the peak at 2θ = 34° and 36°. The presence of calcium and the potential calcium-based oxide phases is not detected by XRD which can be attributed to the extremely low content of calcium. The normalized intensities of the TID alloys are shown in Table 3. The relative basal intensity is the highest for the 250 °C sample, followed by 200 °C and 300 °C, respectively. It can be noted that the relative intensity corresponding to the pyramidal plane (2θ = 36°) is the maximum for all the TID alloys. This indicates that all the TID alloys have contributed to the weakening of the typical basal texture observed in traditional magnesium and its alloys.

Table 3. Normalized intensities of the TID alloys.

Material	Plane	I/I_{max}
200 °C	10–10 prism	0.16
	0002 basal	0.57
	10–11 pyramidal	1
250 °C	10–10 prism	0.10
	0002 basal	0.83
	10–11 pyramidal	1
300 °C	10–10 prism	0.14
	0002 basal	0.35
	10–11 pyramidal	1

3.3. Thermal Properties

A differential scanning calorimetry (DSC) test was used to determine the transformation temperature of the materials, which was shown in Figure 3. The material had no obvious phase transformation temperature peak during the heating process within the scope of the current research. The solid solubility of zinc in magnesium is very high and

the eutectic composition of the Mg-Zn alloy system is $Mg_{47}Zn_{53}$ (wt. %) [27]. Hence, with the increasing temperature, there were no other phases formed but only the solid solubility of mainly Zn increases gradually.

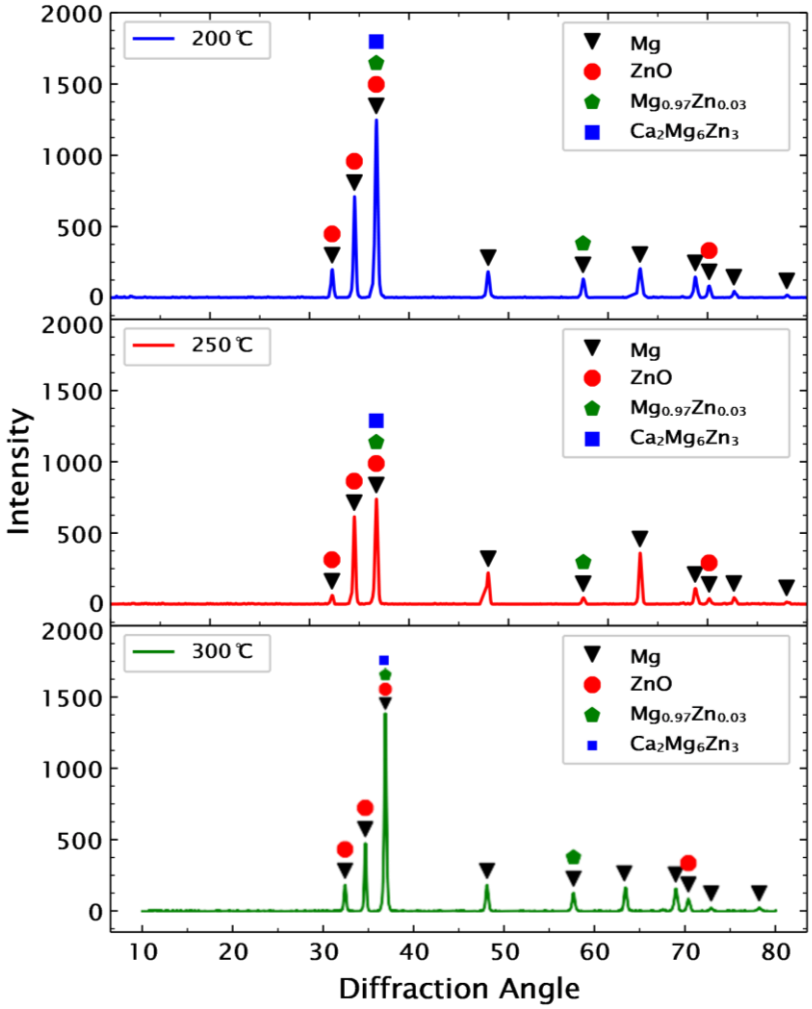

Figure 2. XRD of the TID alloys.

The results of the coefficient of thermal expansion (CTE) are shown in Table 4. The material developed shows excellent thermal stability with a relatively low coefficient of thermal expansion when compared to pure Mg. There was no trend observed as a function of the extrusion temperature; however, the highest extrusion temperature (300 °C) displayed the lowest CTE.

Table 4. Ignition temperature and coefficient of thermal expansion results.

Material	Ignition Temperature (°C)	CTE ($\times 10^{-6}/K$)
Pure Mg	581	27.1
200 °C	601	24.16
250 °C	605	24.39
300 °C	610	23.09

The ignition temperature was determined using a thermogravimetric analyzer and the TGA results are shown in Table 4. The ignition temperature increases with the increase in extrusion temperature. This is due to the formation of thermally stable oxides ZnO, MgO, and CaO during turning, compaction, and extrusion, which increases the ignition

temperature. The extrusion temperature has a slightly positive effect on the ignition temperature. The ignition temperature is related to microscopic properties, such as grain size and porosity [28]. A finer grain size will lead to a lower ignition temperature. In the range of 200–300 °C, the influence of extrusion temperature on ignition temperature is primarily the grain size refinement, considering that the porosities are minimal. It is worth noting that the ignition temperature of the materials processed by TID technology is significantly higher than that of pure Mg (580 °C), AZ61 (559 °C), AZ91 (600 °C), and lower than AZ31 (628 °C) [29].

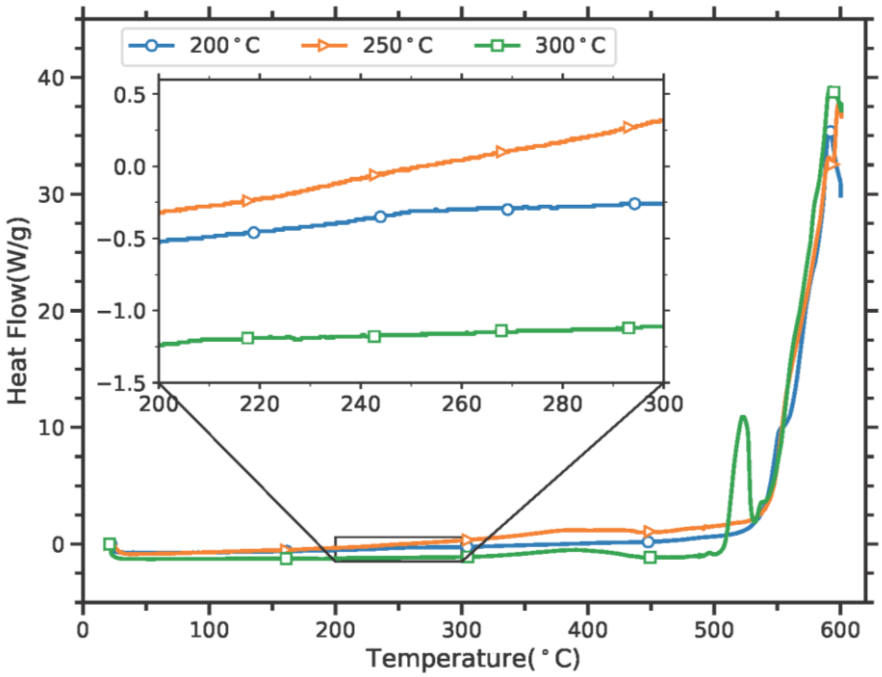

Figure 3. Heat flow vs. temperature from DSC test. The relationship graph within the whole testing process and the inset graph is within the scope of current research.

3.4. Mechanical Properties

The microhardness testing results are shown in Table 5. The microhardness of the alloys processed using the TID technique is comparable within the error range to that of the no-TID alloy, and the effect of extrusion temperature on microhardness was found to be negligible. Microhardness is related to composition and microstructure (such as grain size, the bond between chips and the shape, size, and distribution of the secondary phases) [30,31]. This indicates that the overall microstructural variations during TID do not alter the response of the alloys to localized plastic deformation.

Table 5. Microhardness results.

Processing Conditions	Hardness (HV)
No TID (250 °C)	91 ± 4
200 °C	89 ± 4
250 °C	89 ± 4
300 °C	93 ± 8

Figure 4 is the engineering stress-strain curve of each specimen, and the summary of the test results of the specimen is shown in Table 6. The compression results reveal no particular trend as a function of the extrusion temperature. Compared to the No-TID sample extruded at 250 °C, compressive yield strength (0.2% CYS) reduced, and ultimate compressive strength (UCS) increased while the fracture strain remained similar for all the TID alloys.

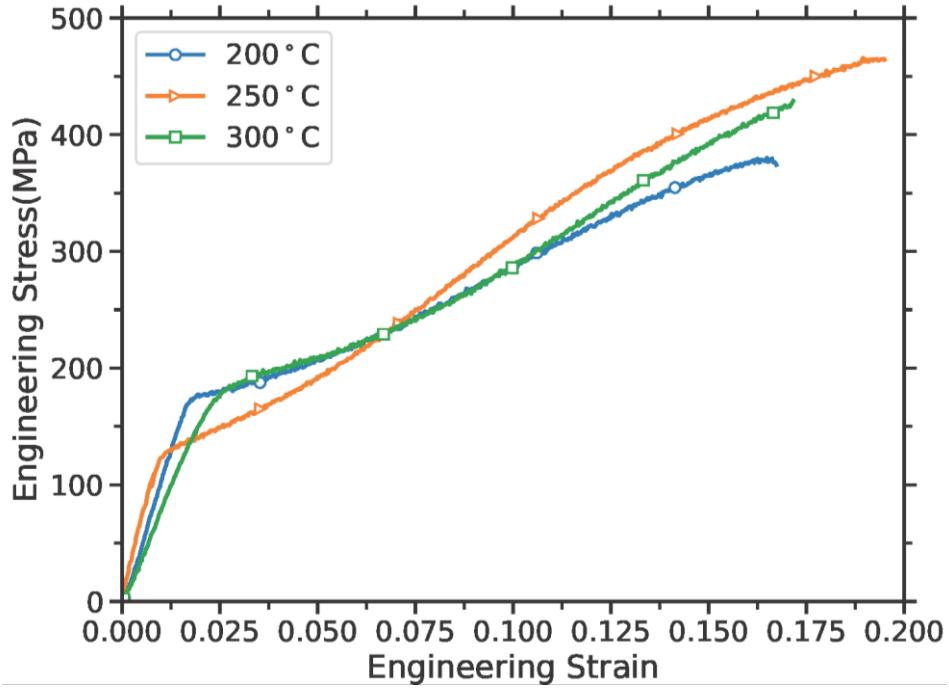

Figure 4. Engineering stress-strain graph for TID alloys.

The compression test results indicate that at a 250 °C extrusion temperature, which is beyond the recrystallization temperature of magnesium, the dynamic recrystallization occurs during the extrusion process leading to a dominant grain refining effect, and the friction stresses necessary to initiate the dislocation motion subsequently reduced [32]. The increase in UCS at 250 °C and 300 °C extrusion temperatures indicate the higher work hardening capability of the alloy owing to the reduction in obstacles to the dislocation motion which appears to be optimal at 250 °C wherein the samples display the highest UCS values. To note that as an orthopedic implant, the plasticity reported in this study is acceptable as it is much superior to that exhibited by the natural bone. From Table 6, it can also be observed that the TID alloys at all extrusion temperatures have comparable yield strength and superior ultimate strength and fracture strain values in comparison with commercial Mg alloys. This validates the use of a hybrid manufacturing process (TID + hot extrusion) to develop magnesium alloys with industrially acceptable properties.

Table 6. Compression test results.

Material	0.2% CYS (MPa)	UCS (MPa)	Fracture Strain (%)
No TID (250 °C)	187 ± 5	420 ± 10	25 ± 2
200 °C	171 ± 6	360 ± 15	18 ± 1
250 °C	123 ± 5	463 ± 19	23 ± 1
300 °C	191 ± 5	426 ± 11	19 ± 1
ME21 (Extruded) [a]	87	260	25
ZK60 (Extruded) [a]	159	472	12.4
WE43 (Extruded) [a]	183	305	11.3
WE54 (Extruded) [a]	210	325	27
AZ31 [a]	-	250	28
AZ91D [a]	130	300	12.4

[a]—[33].

Figure 5 shows the fractography of the cross-section of the compression test specimens. The micro-fracture morphology shows the characteristics of ductile-brittleness mixed fracture. Two regions (rough surfaces and also shear bands) [34] representing different fracture modes can be observed. The region with rough surfaces shows the shear mode of failure is formed by the shearing effect of the zinc oxide phase. Meanwhile, the smooth

region shows a ductile fracture. The presence of the MgZnCa ternary phase acts as an obstacle and the magnesium matrix becomes the crack initiation site during the compression test, where an effective load transfer happens between the softer magnesium matrix and the harder MgZnCa phase [35].

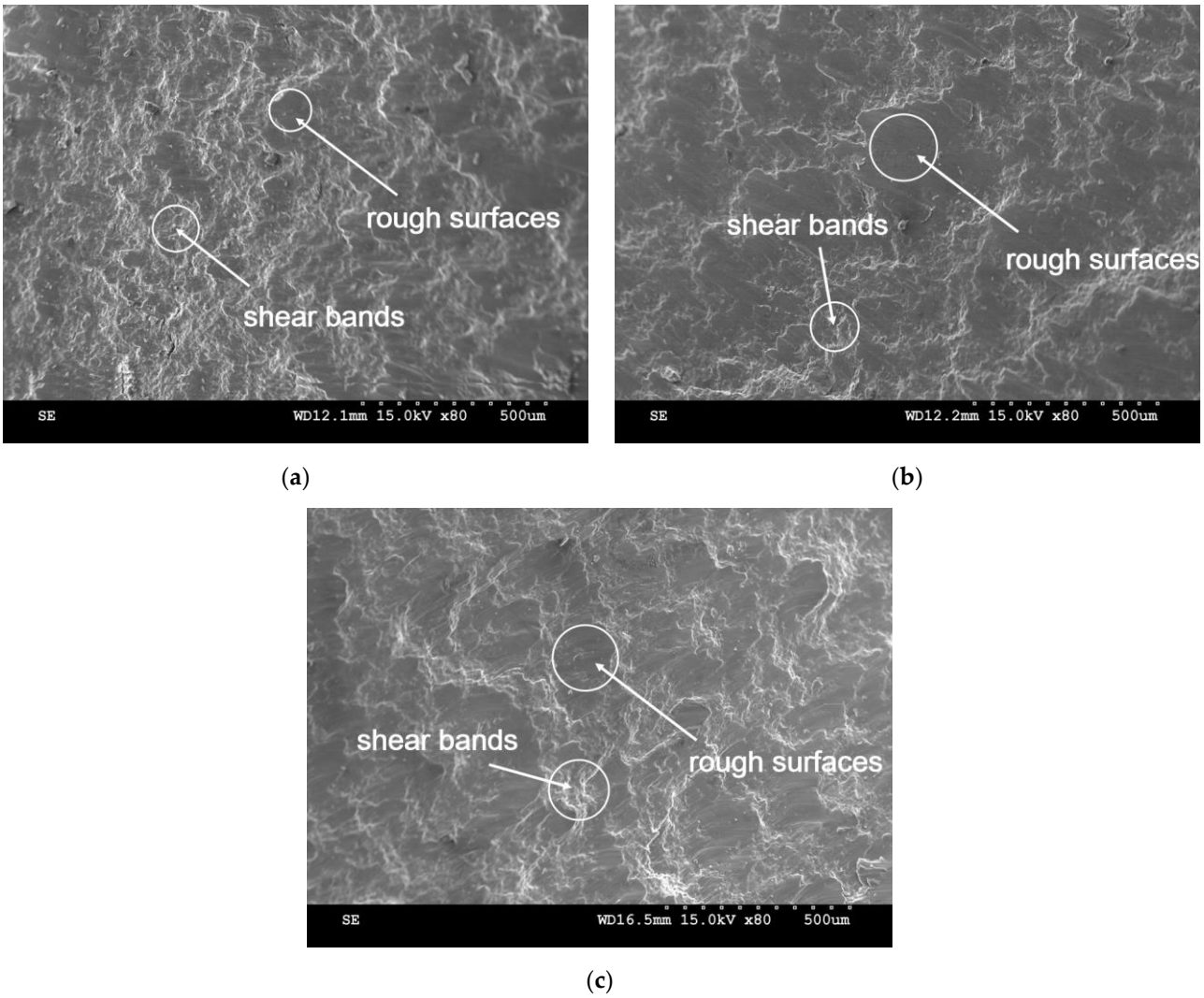

Figure 5. FESEM graph of compression test fracture surface (**a**) 200 °C, (**b**) 250 °C, (**c**) 300 °C. The length scales are in μm.

3.5. Damping Characteristics

The rate at which the attenuation (α) of the sound wave occurs or the consumption of the sound wave energy is defined as the damping capacity of a material. A material with a higher damping capacity possesses a higher internal friction coefficient, therefore rapidly absorbing the sound wave energy. The elastic modulus of the material determines the amount of internal friction it retains. The lower the elastic modulus, the higher the internal friction. The amplitude of the vibration signal at any time t is given by the following Equation (1) [36]:

$$A(t) = A(0)e^{(-(\alpha)t)} + C \quad (1)$$

where α is the attenuation coefficient.

The damping test results are shown in Table 7 and Figure 6. With the increase in extrusion temperature, damping capacity, loss rate, and attenuation coefficient all showed a decreasing trend, which indicates that the sample prepared at a lower extrusion temperature has a better damping performance. Comparing the materials prepared at 250 °C with that

at 200 °C, the damping capacity, loss rate and attenuation coefficient reduced by ~19%, ~21%, and ~9%, respectively. Similarly, comparing the materials prepared at 300 °C with that at 250 °C, the damping capacity, loss rate, and attenuation coefficient reduced by ~8%, ~8%, and ~25%, respectively. The increasing extrusion temperature shows a negative effect on the loss rates, damping capacity, and attenuation coefficients. The damping properties are closely related to the motion of dislocations within the material [37]. The thermal mismatch, dislocation, defects, and porosity [38] obstruct dislocation movement via different mechanisms that help to dissipate cyclic loading energy as thermal energy. The increased extrusion temperature leads to the growth of the grain boundary, which reduces the resistance to dislocation movement. However, the porosity shows a positive relationship with extrusion temperature, which has a positive impact on the damping properties. The results showed that the reduction in grain size is dominant in the balance between the two mechanisms.

Table 7. Damping and Young's modulus results.

Material	Damping Capacity (Ns/mm)	Loss Rate	Attenuation Coefficient (α)	Elastic Modulus (GPa)
No TID (250 °C)	0.471 ± 0.093	17.5 ± 2.61	19.38	45.30 ± 0.72
200 °C	0.590 ± 0.062	23.24 ± 2.44	22.77	42.89 ± 0.28
250 °C	0.475 ± 0.044	18.19 ± 1.69	20.66	44.18 ± 0.08
300 °C	0.433 ± 0.030	16.62 ± 1.15	15.36	43.34 ± 0.02
MA21 [b]				45
MA18 [b]				45
LA141 [b]				43
AZ31B [b]				46
AM60 [b]		-		45
Al2024 [b]				74
Al6061 [b]				73
T4C titanium alloy [b]				110
45 steel [b]				200

[b]—[33].

3.6. Biocorrosion

In a bio-simulated environment, pitting and galvanic corrosion are the main mechanisms in the corrosion process of magnesium alloy. Research shows that due to the electro-potential difference between Zn, Mg matrix and the second phase (excess zinc precipitated during solution), the galvanic cell is formed, leading to pitting at the second phase position [39,40]. At the initial stage of the reaction, the alloy reacted with HBSS, and the magnesium dissolves to form magnesium cations (Mg^{2+}) and simultaneously produces hydrogen and a large number of hydroxyl ions (OH^-). This increased the pH of the solution, and hydroxyapatite formed and precipitated onto the surface of the alloy, which prevented further corrosion and decreases the corrosion rate [41,42]. However, possible mechanical wear in the human body environment would damage the protective film, causing rapid corrosion of the exposed site and also leaving exfoliated debris, which would lead to abrasive wear [43].

The magnesium corrosion mechanism can be briefly summarized by Equations (2)–(4).

$$Mg = Mg^{2+} + 2e^-, \quad \text{Anodic reaction} \tag{2}$$

$$2H^+ + 2e^- = H_2, \quad \text{Cathodic reaction} \tag{3}$$

$$Mg^{2+} + 2OH^- = Mg(OH)_2 \tag{4}$$

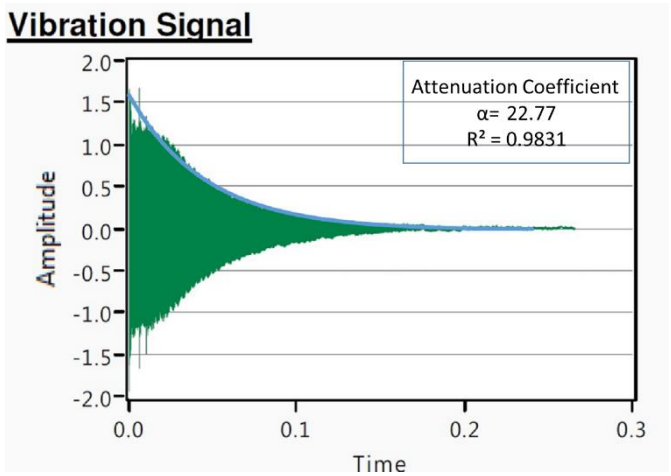

(**a**)

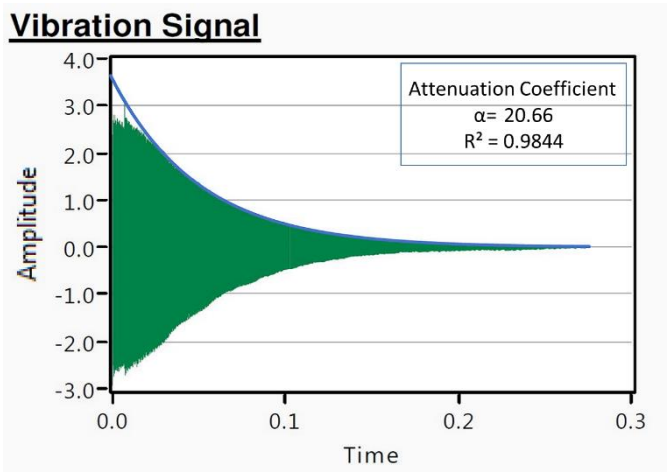

(**b**)

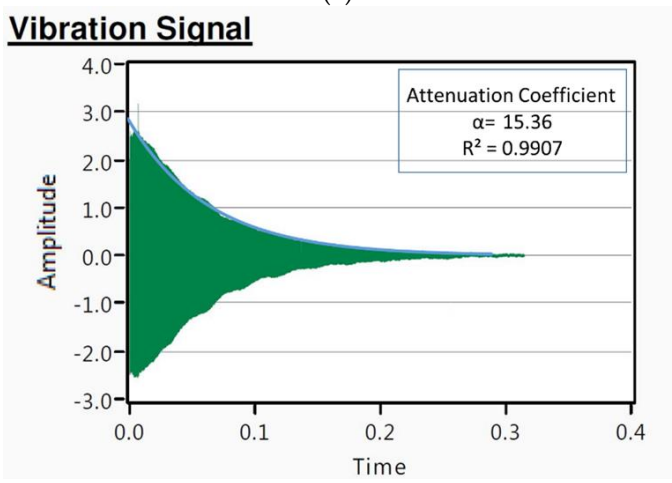

(**c**)

Figure 6. Damping plots and attenuation coefficient of the materials. (**a**) 200 °C, (**b**) 250 °C, (**c**) 300 °C.

The testing results are shown in Table 8. The increasing extrusion temperature has a negative impact on the corrosion resistance of materials at the end of day eight. The residual strain caused by the deformation of materials during TID processing will also increase the pitting sensitivity [44]. In addition, the corrosion process might be accelerated due to the exposure of vulnerable sections of the sample and a large cathode surface area consisting of zinc oxide. Hence, porosity is another major factor affecting the corrosion resistance of alloys. However, good porosity can improve biocompatibility and biodegradability when applied to orthopedic implants. Compared with some common materials in Table 9, TID-processed Mg-4Zn-1Ca alloy shows acceptable corrosion resistance, which indicates its potential for applications as a biomaterial. The corrosion rate of the material in millimeters per year (mm/y) can be calculated using the following Equation (5): [45]

$$CR = \frac{(K \times W)}{(A \times T \times D)} \quad (5)$$

where time conversion coefficient, $K = 8.76 \times 10^4$, W is the change in weight pre- and post-immersion (g), A is the surface area of the cylinder exposed to the immersive medium (cm^2), T is the time of immersion (h), and D is the experimental density of the material (g/cm^3). Conversion coefficient 'K' is used to convert the corrosion rate values from cm/h to mm/y.

Table 8. Corrosion rate (mm/y) results.

Material	200 °C	250 °C	300 °C
0	0.00	0.00	0.00
1	0.43	1.16	0.92
2	0.36	1.58	0.86
3	0.38	2.86	0.95
8	1.81	4.06 *	4.12 *

*—Sample degraded completely.

Table 9. Comparison of corrosion rates (mm/y) of the different Mg alloys on day 3.

Material	Corrosion Rate (mm/y)	Material	Corrosion Rate (mm/y)
Mg-4Zn-1Ca (200 °C)	0.38	Mg1Ca3Zn [c]	2.92
Mg-4Zn-1Ca (250 °C)	2.86	Mg5Zn [c]	2.25
Mg-4Zn-1Ca (300 °C)	0.95	Mg5Zn0.2Sr [c]	1.75
Mg1Ca1Zn [c]	2.13	Mg3Sr [c]	0.75
Pure Mg [c]	2.08	ZE41 [c]	2.04
Mg1Ca [c]	3.16	AZ91 [c]	3.56

[c]—[45].

The 250 °C sample has the highest corrosion rate at the end of day three, which is probably attributed to the combination of microstructure and the typical texture the sample exhibited. In the case of the 200 °C and 300 °C samples, it is observed that there is a drop in the corrosion rate on day 2 and a slight increase at the end of day 3, which can be attributed to the protective hydroxide layer which was formed by the reaction between Mg^{2+} ions dissolved in the solution and the free OH^- ions. The corrosion rate rises steeply for all the samples except for the 200 °C sample where there is a relatively lower rise from day 3 to day 8. The 250 °C samples and the 300 °C samples were completely corroded after 8 days. It can be concluded that higher extrusion temperatures led to poorer corrosion resistance. The fine-grained structure promotes the formation of a more protective surface film.

4. Conclusions

- In this study, near-dense Mg-4Zn-1Ca alloys were successfully synthesized using the sinterless turning-induced deformation method. The elimination of the sintering step can have far-reaching implications for reducing the cost of the end product.
- In general, TID displayed the ability to refine the microstructure of the Mg-4Zn-1Ca alloy. At a lower extrusion temperature of 200 °C, the grain refinement was observed to be significant in comparison to that at 250 °C and 300 °C.
- There is a clear trend observed in the thermal stability of the materials, wherein the resistance to auto-ignition increased linearly with increasing extrusion temperatures. The lowest coefficient of thermal expansion was exhibited by the 300 °C extruded samples.
- The 300 °C extruded samples displayed the highest yield strength properties, while the 250 °C extruded samples showed the highest ultimate strength and fracture strain values.
- Damping characteristics were observed to be the best at 200 °C extruded samples and a decrease with respect to the increased extrusion temperature was observed.
- The corrosion rate of the TID alloys increases with the increase in extrusion temperature with 200 °C extruded samples displaying the maximum corrosion resistance.

Author Contributions: Conceptualization, G.P. and M.G.; methodology, M.G.; validation, Z.W., G.P. and M.G.; formal analysis, Z.W. and G.P.; investigation, Z.W.; resources, M.G.; data curation, Z.W. and G.P.; writing—original draft preparation, Z.W., G.P. and M.G.; writing—review and editing, Z.W., G.P. and M.G.; visualization, Z.W. and G.P.; supervision, G.P. and M.G.; project administration, M.G.; funding acquisition, M.G. All authors have read and agreed to the published version of the manuscript.

Funding: This research was funded by the Singapore Ministry of Education Academic Research Fund Tier 1 project with grant number R-265-000-684-114 (A-0005234-01-00) and the APC was funded by R-265-000-684-114 (A-0005234-01-00).

Data Availability Statement: Data will be made available on request.

Conflicts of Interest: The authors declare no conflict of interest. The funders had no role in the design of the study; in the collection, analyses, or interpretation of data; in the writing of the manuscript; or in the decision to publish the results.

References

1. Dziubińska, A.; Gontarz, A.; Dziubiński, M.; Barszcz, M. The forming of magnesium alloy forgings for aircraft and automotive applications. *Adv. Sci. Technol. Res. J.* **2016**, *10*, 158–168. [CrossRef]
2. Joost, W.J.; Krajewski, P.E. Towards magnesium alloys for high-volume automotive applications. *Scr. Mater.* **2017**, *128*, 107–112. [CrossRef]
3. Maier, P.; Hort, N. Magnesium Alloys for biomedical applications. *Metals* **2020**, *10*, 1328. [CrossRef]
4. Teo, Z.M.B.; Parande, G.; Manakari, V.; Gupta, M. Using low-temperature sinterless powder method to develop exceptionally high amount of zinc containing Mg–Zn–Ca alloy and Mg–Zn–Ca/SiO_2 nanocomposite. *J. Alloys Compd.* **2021**, *853*, 156957. [CrossRef]
5. Prasadh, S.; Ratheesh, V.; Manakari, V.; Parande, G.; Gupta, M.; Wong, R. The Potential of Magnesium Based Materials in Mandibular Reconstruction. *Metals* **2019**, *9*, 302. [CrossRef]
6. Prasad, S.V.S.; Prasad, S.B.; Verma, K.; Mishra, R.K.; Kumar, V.; Singh, S. The role and significance of Magnesium in modern day research-A review. *J. Magnes. Alloy.* **2022**, *10*, 1–61. [CrossRef]
7. Parande, G.; Manakari, V.; Prasadh, S.; Chauhan, D.; Rahate, S.; Wong, R.; Gupta, M. Strength retention, corrosion control and biocompatibility of Mg–Zn–Si/HA nanocomposites. *J. Mech. Behav. Biomed. Mater.* **2020**, *103*, 103584. [CrossRef]
8. Nakamura, Y.; Tsumura, Y.; Tonogai, Y.; Shibata, T.; Ito, Y. Differences in behavior among the chlorides of seven rare earth elements administered intravenously to rats. *Toxicol. Sci.* **1997**, *37*, 106–116. [CrossRef]
9. Yang, L.; Zhang, E. Biocorrosion behavior of magnesium alloy in different simulated fluids for biomedical application. *Mater. Sci. Eng. C* **2009**, *29*, 1691–1696. [CrossRef]
10. Zhao, L.-Q.; Wang, C.; Chen, J.-C.; Ning, H.; Yang, Z.-Z.; Xu, J.; Wang, H.-Y. Development of weak-textured and high-performance Mg–Zn–Ca alloy sheets based on Zn content optimization. *J. Alloys Compd.* **2020**, *849*, 156640. [CrossRef]
11. Zhou, M.; Huang, X.; Morisada, Y.; Fujii, H.; Chino, Y. Effects of Ca and Sr additions on microstructure, mechanical properties, and ignition temperature of hot-rolled Mg–Zn alloy. *Mater. Sci. Eng. A* **2020**, *769*, 138474. [CrossRef]
12. Duley, P.; Bairagi, D.; Bairi, L.R.; Bandyopadhyay, T.K.; Mandal, S. Effect of microstructural evolution and texture change on the in-vitro bio-corrosion behaviour of hard-plate hot forged Mg-4Zn-0.5Ca-0.16Mn (wt%) alloy. *Corros. Sci.* **2021**, *192*, 109860. [CrossRef]
13. Jin, Y.; Blawert, C.; Yang, H.; Wiese, B.; Feyerabend, F.; Bohlen, J.; Mei, D.; Deng, M.; Campos, M.S.; Scharnagl, N.; et al. Microstructure-corrosion behaviour relationship of micro-alloyed Mg-0.5Zn alloy with the addition of Ca, Sr, Ag, In and Cu. *Mater. Des.* **2020**, *195*, 108980. [CrossRef]
14. Wang, J.; Ma, Y.; Guo, S.; Jiang, W.; Liu, Q. Effect of Sr on the microstructure and biodegradable behavior of Mg–Zn–Ca-Mn alloys for implant application. *Mater. Des.* **2018**, *153*, 308–316. [CrossRef]
15. Danish, M.; Yasir, M.; Mia, M.; Nazir, K.; Ahmed, T.; Rani, A.M.A. High speed machining of magnesium and its alloys. In *High Speed Machining*; Gupta, K., Paulo Davim, J., Eds.; Academic Press: Cambridge, MA, USA, 2020; pp. 263–282. [CrossRef]
16. Shi, K.; Zhang, D.; Ren, J.; Yao, C.; Huang, X. Effect of cutting parameters on machinability characteristics in milling of magnesium alloy with carbide tool. *Adv. Mech. Eng.* **2016**, *8*, 1687814016628392. [CrossRef]
17. Akyuz, B. Machinability of magnesium and its alloys. *TOJSAT* **2011**, *1*, 31–38.
18. Johanes, M.; Gupta, M. The Promise of Turning Induced Deformation Process for Synthesizing Magnesium Based Materials with Superior Mechanical Response. *Technologies* **2021**, *9*, 69. [CrossRef]
19. Tekumalla, S.; Gupta, N.; Gupta, M. Influence of turning speed on the microstructure and properties of magnesium ZK60 alloy pre-processed via turning-induced-deformation. *J. Alloys Compd.* **2020**, *831*, 154840. [CrossRef]
20. Tekumalla, S.; Ajjarapu, M.; Gupta, M. A Novel Turning-Induced-Deformation Based Technique to Process Magnesium Alloys. *Metals* **2019**, *9*, 841. [CrossRef]
21. Wan, B.; Chen, W.; Lu, T.; Liu, F.; Jiang, Z.; Mao, M. Review of solid state recycling of aluminum chips. *Resour. Conserv. Recycl.* **2017**, *125*, 37–47. [CrossRef]

22. Kujur, M.S.; Manakari, V.; Parande, G.; Prasadh, S.; Wong, R.; Mallick, A.; Gupta, M. Development of rare-earth oxide reinforced magnesium nanocomposites for orthopaedic applications: A mechanical/immersion/biocompatibility perspective. *J. Mech. Behav. Biomed. Mater.* **2021**, *114*, 104162. [CrossRef] [PubMed]
23. Yu, Z.; Chen, J.; Yan, H.; Xia, W.; Su, B.; Gong, X.; Guo, H. Degradation, stress corrosion cracking behavior and cytocompatibility of high strain rate rolled Mg-Zn-Sr alloys. *Mater. Lett.* **2020**, *260*, 126920. [CrossRef]
24. Matsubara, K.; Miyahara, Y.; Horita, Z.; Langdon, T. Developing superplasticity in a magnesium alloy through a combination of extrusion and ECAP. *Acta Mater.* **2003**, *51*, 3073–3084. [CrossRef]
25. Sellars, C. Recrystallization of metals during hot deformation. *Philos. Trans. R. Soc. Lond. Ser. A Math. Phys. Sci.* **1978**, *288*, 147–158.
26. Roostaei, M.; Shirdel, M.; Parsa, M.; Mahmudi, R.; Mirzadeh, H. Microstructural evolution and grain growth kinetics of GZ31 magnesium alloy. *Mater. Charact.* **2016**, *118*, 584–592. [CrossRef]
27. Mezbahul-Islam, M.; Mostafa, A.; Medraj, M. Essential magnesium alloys binary phase diagrams and their thermochemical data. *J. Mater.* **2014**, *2014*, 704283. [CrossRef]
28. Tekumalla, S.; Si Chun, L.; Gupta, M. Preprocessing of powder to enhance mechanical and thermal response of bulk magnesium. *Met. Powder Rep.* **2019**, *74*, 137–140. [CrossRef]
29. Tekumalla, S.; Gupta, M. An insight into ignition factors and mechanisms of magnesium based materials: A review. *Mater. Des.* **2017**, *113*, 84–98. [CrossRef]
30. Anilchandra, A.; Surappa, M. Microstructure and damping behaviour of consolidated magnesium chips. *Mater. Sci. Eng. A* **2012**, *542*, 94–103. [CrossRef]
31. Krystýnová, M.; Doležal, P.; Fintová, S.; Březina, M.; Zapletal, J.; Wasserbauer, J. Preparation and characterization of zinc materials prepared by powder metallurgy. *Metals* **2017**, *7*, 396. [CrossRef]
32. Yang, W.; Tekumalla, S.; Gupta, M. Cumulative effect of strength enhancer—Lanthanum and ductility enhancer—Cerium on mechanical response of magnesium. *Metals* **2017**, *7*, 241. [CrossRef]
33. Mishra, S.K.; Manakari, V.; Parande, G.; Matli, P.R.; Gupta, M. Development of Ultralight Binary Mg-Li Alloys: Enhancing Damping, Ductility, and Ultimate Compressive Strength beyond 2000 MPa. *J. Mater. Eng. Perform.* **2022**. [CrossRef]
34. Tun, K.S.; Wong, W.L.E.; Nguyen, Q.B.; Gupta, M. Tensile and compressive responses of ceramic and metallic nanoparticle reinforced Mg composites. *Materials* **2013**, *6*, 1826–1839. [CrossRef]
35. Medina, J.; Garces, G.; Pérez, P.; Stark, A.; Schell, N.; Adeva, P. High temperature mechanical behaviour of Mg–6Zn–1Y alloy with 1 wt.% calcium addition: Reinforcing effect due to I-(Mg3Zn6Y1) and Mg6Zn3Ca2 phases. *J. Magnes. Alloy.* **2020**, *8*, 1047–1060. [CrossRef]
36. Parande, G.; Manakari, V.; Sharma Kopparthy, S.D.; Gupta, M. A study on the effect of low-cost eggshell reinforcement on the immersion, damping and mechanical properties of magnesium–zinc alloy. *Compos. Part B Eng.* **2020**, *182*, 107650. [CrossRef]
37. Zhang, J.; Perez, R.; Lavernia, E. Dislocation-induced damping in metal matrix composites. *J. Mater. Sci.* **1993**, *28*, 835–846. [CrossRef]
38. Kumar, A.; Meenashisundaram, G.K.; Manakari, V.; Parande, G.; Gupta, M. Lanthanum effect on improving CTE, damping, hardness and tensile response of Mg-3Al alloy. *J. Alloys Compd.* **2017**, *695*, 3612–3620. [CrossRef]
39. Zhang, B.; Hou, Y.; Wang, X.; Wang, Y.; Geng, L. Mechanical properties, degradation performance and cytotoxicity of Mg–Zn–Ca biomedical alloys with different compositions. *Mater. Sci. Eng. C* **2011**, *31*, 1667–1673. [CrossRef]
40. Prasadh, S.; Parande, G.; Gupta, M.; Wong, R. Compositional Tailoring of Mg–2Zn–1Ca Alloy Using Manganese to Enhance Compression Response and In-Vitro Degradation. *Materials* **2022**, *15*, 810. [CrossRef]
41. Xin, Y.; Hu, T.; Chu, P.K. Influence of test solutions on in vitro studies of biomedical magnesium alloys. *J. Electrochem. Soc.* **2010**, *157*, C238. [CrossRef]
42. Xin, Y.; Huo, K.; Hu, T.; Tang, G.; Chu, P.K. Corrosion products on biomedical magnesium alloy soaked in simulated body fluids. *J. Mater. Res.* **2009**, *24*, 2711–2719. [CrossRef]
43. Li, H.; Liu, D.; Zhao, Y.; Jin, F.; Chen, M. The influence of Zn content on the corrosion and wear performance of Mg-Zn-Ca alloy in simulated body fluid. *J. Mater. Eng. Perform.* **2016**, *25*, 3890–3895. [CrossRef]
44. Chen, H.; Lu, L. Effect of residual stress on localized corrosion behavior of metallic materials. *Chin. J. Eng.* **2019**, *41*, 929. [CrossRef]
45. Parande, G.; Manakari, V.; Gupta, H.; Gupta, M. Magnesium-β-Tricalcium Phosphate Composites as a Potential Orthopedic Implant: A Mechanical/Damping/Immersion Perspective. *Metals* **2018**, *8*, 343. [CrossRef]